JACS
JOURNAL OF THE AMERICAN CHEMICAL SOCIETY

Article

pubs.acs.org/JACS

Chirality Control for in Situ Preparation of Gold Nanoparticle Superstructures Directed by a Coordinatable Organogelator

Liangliang Zhu,[†,§] Xin Li,[‡,§] Shaojue Wu,[†] Kim Truc Nguyen,[†] Hong Yan,[†] Hans Ågren,[‡] and Yanli Zhao*[,†,∥]

[†]Division of Chemistry and Biological Chemistry, School of Physical and Mathematical Sciences, Nanyang Technological University, 21 Nanyang Link, Singapore 637371

[‡]Department of Theoretical Chemistry and Biology, School of Biotechnology, KTH Royal Institute of Technology, SE-10691 Stockholm, Sweden

[∥]School of Materials Science and Engineering, Nanyang Technological University, 50 Nanyang Avenue, Singapore 639798

Supporting Information

ABSTRACT: Imposing chirality into nanoscale superstructures is a major step forward toward systematic understanding and utilization of nanomaterials. In an attempt to achieve tunable chirality during in situ preparation of hybrid nanomaterials, we here report a novel unimolecular strategy of employing a coordinatable organogelator for the realization of chirality control in the formation of gold nanoparticle superstructures. The work takes advantage of thermally reversible sol−gel transition of the chiral dispersion as template, which causes different micelle properties that can influence the coordination ability between the organogelator and Au(III) ions. Followed by a reduction reaction, gold nanoparticle superstructures with *P*-helicity were prepared from the sol form of the template through a coordination-induced chiral inversion, whereas those with *M*-helicity were obtained from the gel form with chiral holding. Such superstructures are solvent-stable and the chirality difference between them could be observed in many solvent environments.

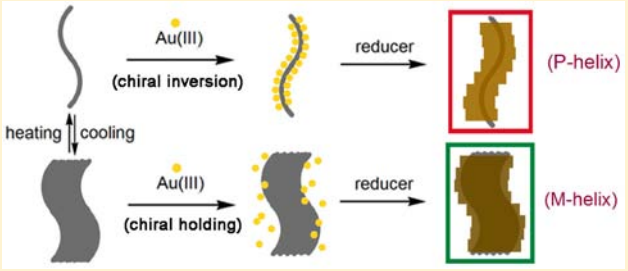

INTRODUCTION

Chirality has become a very important topic in nanoscience since a chiral nano-object generally presents distinct properties from those of the individual subunits or building blocks.[1] In particular, chiral hybrid nanomaterials having structure-specific stability and morphological diversity exhibit promising potentials for applications in asymmetric catalysis, selective separation, chiral sensing, and novel photonics.[2] The past decade has witnessed extensive progress in the nanoengineering of chiral composite nanomaterials,[3] where a typical approach developed thus far to impart chirality into nanoarchitectures is to employ organic chiral molecules, for example, specifically designed peptides,[4] DNAs,[5] surfactants,[6] sol−gel systems,[7] etc.,[8] as template ligands or intermediates to be incorporated with inorganic counterparts. However, facile tuning of chirality in these materials is still difficult, and conformational alterations for most of the superstructures are not readily accessible. To the best of our knowledge, intentional control of chirality has largely relied on either the employment of different enantiomer templates[9] or the assistance of specific treatments.[10] A straightforward approach for the control of chiral expressions in an in situ preparation process remains a challenge.

On this basis, we propose a unimolecular strategy of harnessing controllable interactions between functional organic chiral template and the inorganic counterpart during the preparation process for realization of the hypotheses. The strategy is inspired by the chirality regulation of self-assembled organic structures via certain external stimuli,[11] especially by the coordination-induced structural transformation.[12] Our idea is to employ the coordination approach to aid our design and meanwhile to make use of an orthogonal factor (i.e., temperature) for the modulation of ordered self-assembly properties through selective control of the coordination effect.

Thus, a novel organogelator was designed and synthesized by covalently incorporating lipoic acid, azobenzene, and cholesterol into a unimolecular platform (compound SAC, see Figure 1). Cholesterol is a highly efficient initiator for the construction of chiral low-molecular-weight organogels.[13] Azobenzene is well-known for its photochemical characteristics,[14] redox properties,[15] and the coordination ability toward heavy metal species like auric chloride.[16] It can also serve as a chromophore label for the chiroptical outputs in this work.[13] The disulfide unit has a very high affinity for the surfaces of many inorganic materials.[17] Overall, the preparation of hybrid gold nanomaterials was designed to take advantage of the Au(III)−azo coordination as well as the gold−thiol binding.[18] With these functions in mind, we envision that a chiral sol−gel system may

Received: April 15, 2013
Published: May 24, 2013

   dx.doi.org/10.1021/ja403722t | *J. Am. Chem. Soc.* 2013, 135, 9174−9180

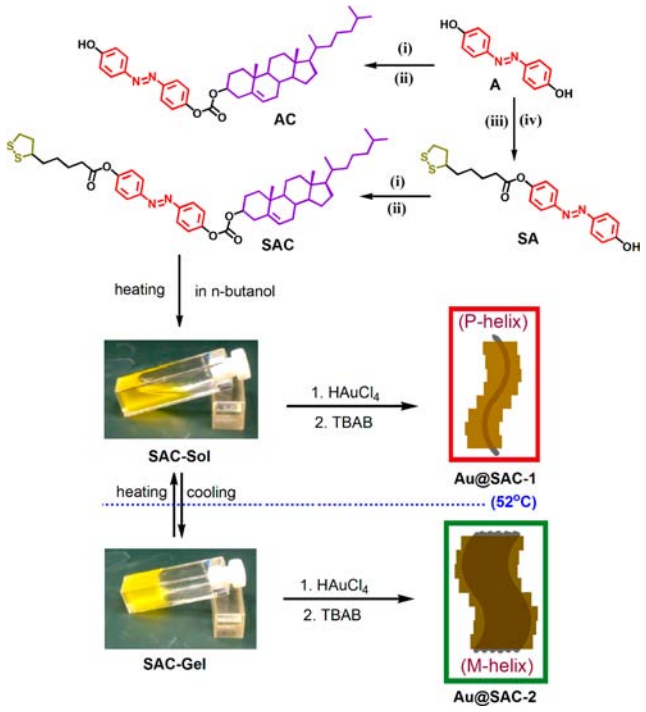

Figure 1. Chemical structures and synthetic routes of SAC, photographs of thermoreversible sol–gel transition of SAC in *n*-butanol, and representation of chirality control in the in situ preparations of SAC-based gold nanoparticle hybrid superstructures via corresponding micelle template. The superstructure Au@SAC-1 with *P*-helicity is prepared from the sol state (SAC-sol) through a chiral inversion, whereas the superstructure Au@SAC-2 with *M*-helicity is prepared from the gel state (SAC-gel) with chiral holding. Reagents and conditions: (i) cholesteryl chloroformate; (ii) triethylamine; (iii) (±)-α-lipoic acid; (iv) 4-(dimethylamino)pyridine and dicyclohexylcarbodiimide.

be formed based on SAC and that the micelles of SAC could be purposely used for the in situ construction of hybrid gold nanoarchitectures under different temperatures with the synergy of coordination reactions.

The synthetic route for preparation of SAC is outlined in Figure 1 (see Experimental Section for synthesis details). The intermediate compounds SA (azobenzene coupled with lipoic acid) and AC (azobenzene conjugated with cholesterol) were used as reference molecules for control studies. It has been well documented that superstructures involving gold nanoparticles possess fascinating plasmonic properties and promising supportive features.[19] In this way, it is necessary to employ a series of characterization techniques to investigate the in situ preparation process as well as chirality control.

RESULTS AND DISCUSSION

Gelation and Sol–Gel Transition. The solvent selectivity for the gelation of SAC was investigated first by circular dichroism (CD) spectroscopy, since it is an effective methodology to probe nanoscale chiral characteristics.[20] Cotton effects of a strong positive CD signal at ~300 nm and a negative one at ~350 nm, corresponding to the electronic transition of the azobenzene unit, were observed when SAC was dispersed in *n*-butanol at a relatively low concentration (Figure 2). Since there is no CD signal observed from the cholesterol unit itself in the spectral region above 250 nm, this phenomenon indicates that the macrochirality of the achiral azobenzene skeleton emerges

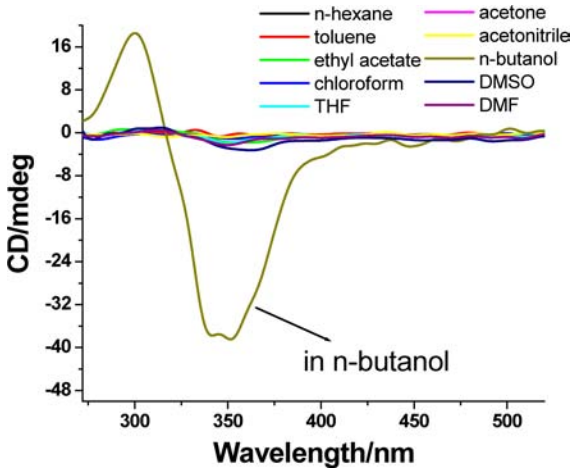

Figure 2. Solvent selectivity for micelle formation: CD spectra of SAC dissolved in different solvents. These spectra were determined at a concentration of 0.03 mM calculated from the azobenzene unit in a cuvette with path length 10 mm at 298 K.

upon the formation of the helically self-assembled nanostructures in a counterclockwise fashion (*M*-helicity). The self-assembly properties of SAC were examined by the absorption variation upon the concentration change. The critical aggregation concentration (cac) of SAC in *n*-butanol was determined to be 10.5 μM (Figure S1a in Supporting Information), and the aggregates formed exhibit a fiber-shaped morphology as visualized by transmission electron microscopy (TEM) (Figure S2 in Supporting Information). SAC is prone to be monodispersed in other organic solvents since no obvious CD signals were observed (Figure 2). The critical micelle concentration (cmc) of this kind of organogelators is usually 1 or 2 orders of magnitude higher than the corresponding cac.[21] In this way, the cmc of SAC was also determined as 420 μM (Figure S1b in Supporting Information).

SAC can completely gelate *n*-butanol above a certain concentration regarded as the critical gelation concentration (cgc = ~0.3 wt %; Figure S3 in Supporting Information) at room temperature. To ensure a favorable condition for phase transition, a sol–gel system with a moderate concentration of SAC (~0.5 wt %) was optimized for the following experiments. The gel-to-sol transition temperature at this concentration is 52 °C. Similar to most other low-molecular-weight gelators,[22] the sol state (SAC-sol) can be reversibly changed into its corresponding gel state (SAC-gel) by cooling it to room temperature and returned to the sol state by heating (Figure 1). In our experiments, the micelles self-assembled from SAC always display a counterclockwise helicity as indicated by the Cotton effects in Figure 2 and Figure S4 in Supporting Information, which is attributed to the molecular structure itself and the sol–gel preparation procedure.[23] The helical self-assembly was prone to be disordered or dissociated upon increasing the temperature, and the CD signal intensity of SAC was reduced accordingly (Figure S4 in Supporting Information). Therefore, temperature can serve as an orthogonal factor to aid in the preparations of helical self-assembly as well as the chirality control.

Coordination-Induced Chiral Inversion. To shed light on the correlation between micelle formation and chirality tuning, we turned to explore the interaction between the micelle template and Au(III) ions. When $HAuCl_4$ was

dx.doi.org/10.1021/ja403722t | J. Am. Chem. Soc. 2013, 135, 9174–9180

respectively introduced into SAC-sol and SAC-gel, different apparent behavior was observed. The color of SAC-sol immediately turned to red upon the addition of 5 equiv of $HAuCl_4$, and the mixture no longer gelated even upon cooling down to room temperature (vial 1 in Figure 3a). In contrast,

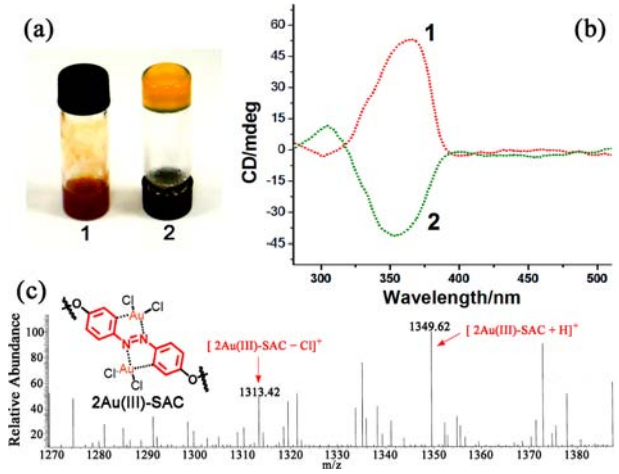

Figure 3. Coordination-induced chiral inversion of the micelle template. (a) Photographs of SAC-sol (vial 1) and SAC-gel (vial 2) after addition of 5 equiv of $HAuCl_4$. (b) CD spectra of *n*-butanol solutions of SAC-sol (curve 1) and SAC-gel (curve 2) after addition of 5 equiv of $HAuCl_4$. (c) ESI-MS spectrum and chemical structure of 2Au(III)−SAC.

the color of SAC-gel slightly changed after the addition of 5 equiv of $HAuCl_4$, and the gel form was preserved after blending and re-gelation (vial 2 in Figure 3a). More interestingly, dilute solutions of the mixtures clearly exhibit chiral differences (see CD spectra in Figure 3b). The Cotton effect of SAC-gel after addition of 5 equiv of $HAuCl_4$ retained a positive−negative pair of peaks from 280 to 400 nm (*M*-helicity),[24] while that of SAC-sol after addition of 5 equiv of $HAuCl_4$ became a negative−positive pair of peaks (*P*-helicity).[24] On the basis of these observations, we infer that a significant interaction between SAC-sol and $HAuCl_4$ is responsible for the chiral inversion. For SAC-gel, the micelles may not get enough contact with $HAuCl_4$ in the gel state, so that the original chirality was kept unchanged.

New absorption bands at around 380 and 470 nm emerged after addition of $HAuCl_4$ into SAC-sol (Figure S5 in Supporting Information). Employing this signal change, we conducted a series of control experiments to investigate the interaction between SAC-sol and $HAuCl_4$. Protonation of SAC was excluded since no absorption change was observed when SAC and excessive trifluoroacetic acid (TFA) are mixed (Table S1 in Supporting Information). The addition of TFA did not influence the chemical structure of SAC under the current experimental conditions. Redox reaction was also ruled out as no cyclic voltammetric (CV) signal was found in the micelle dispersions. As these interactions were excluded, it was inferred that this chiral inversion was caused by coordination of the azobenzene unit with auric chloride, that is, chelation of a phenyl group and a nitrogen atom on the azobenzene unit with $[AuCl_2]$ (see the proposed structure in Figure 3c).[16] Such a coordination site on the azobenzenyl moiety is reasonable since the disulfide unit is prone to bind with Au^0 and Au(I) rather than Au(III). From this aspect, we further explored that SAC is able to coordinate with Au(III) to form a 1:2 complex, 2Au(III)−SAC, in *n*-butanol with a relatively high association constant ($6139 \pm 255\ M^{-2}$) (Figures S6 and S7 in Supporting Information). Electrospray ionization mass spectrometry (ESI-MS) provides additional evidence for formation of the bis-coordinated complex (Figure 3c). Two peaks at m/z = 1313.42 and 1349.62 were observed in the mass spectrum of 2Au(III)−SAC, corresponding to $[M - Cl]^+$ and $[M + H]^+$, respectively. Titration experiments shown in Figure S8 of Supporting Information clearly demonstrate the coordination-induced chiral inversion process.

To gain further insight into the fine superstructures of the aggregates formed from the organogelator and the coordinated complex, we employed molecular dynamics (MD) simulations[25] to study the self-assembly behavior of compounds SAC and 2Au(III)−SAC (see Supporting Information for simulation details). A representative comparison between the *M*- and *P*-helices is shown in Figure 4 by illustrating the stacking patterns

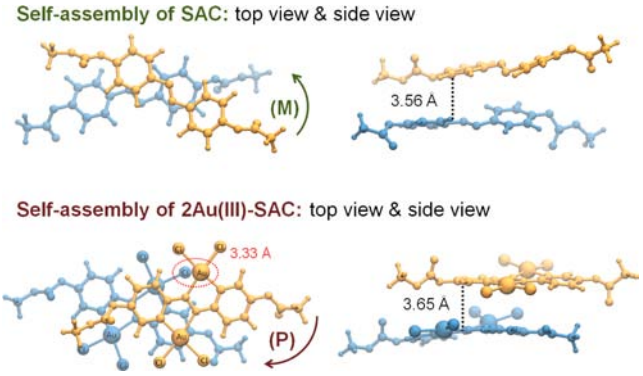

Figure 4. Representative (top) *M*-helical stacking pattern of SAC self-assembly and (bottom) *P*-helical stacking pattern of 2Au(III)−SAC self-assembly, extracted from trajectories of MD simulations.

of the aromatic units in the self-assemblies of SAC and 2Au(III)−SAC, respectively. In the packing mode of SAC, the azobenzenyl unit stacks over the phenyl ring through weak interactions, where the macroscopic helicity is most likely guided by the chiral cholesterol units.[23a] Notably, the stacking pattern and helicity of the 2Au(III)−SAC self-assembly are altered in the presence of gold atoms (Figure 4). Inspection of the intermolecular interaction energies within the self-assemblies (Figure S13 and Table S2 in Supporting Information) indicates that the electrostatic attraction[26] among the 2Au(III)−SAC molecules is significantly enhanced as compared with that in the self-assembly of SAC, due to the presence of gold and chlorine atoms. For both SAC and 2Au(III)−SAC self-assemblies, the vertical distance between two adjacent stacking units is around 3.6 Å, typical of $\pi-\pi$ stacking character, and the relatively short distance between the gold and chlorine atoms (3.33 Å in Figure 4) reflects that the electrostatic attraction takes effect in altering the packing mode and optical rotation of the 2Au(III)−SAC self-assembly.

Chirality Control for in Situ Preparation of Gold Nanoparticle Superstructures. The hybrid gold nanostructures Au@SAC-1 and Au@SAC-2 were prepared from SAC-sol and SAC-gel, respectively, through the addition of $HAuCl_4$ followed by a reduction reaction using tetrabutylammonium borohydride (TBAB) (see Experimental Section for details). Through TEM studies, their superstructure morphologies were observed. Au@SAC-1 with an average cross-sectional diameter of 40 nm tends to curl, whereas Au@SAC-2 with an average

dx.doi.org/10.1021/ja403722t | J. Am. Chem. Soc. 2013, 135, 9174−9180

cross-sectional diameter of 200 nm is relatively widespread (see TEM images in Figure 5 and microscopy images with relatively large scale in Figure 6). In addition, it can be clearly seen from the TEM images that these superstructures were formed through the growth of small gold nanoparticles with diameter less than 5 nm along the micelle surfaces via gold−thiol binding (Figure 5). The distribution of gold nanoparticles in Au@SAC-1 is more compact than that in Au@SAC-2. Formation of the superstructures results in a significantly bathochromic shift of their surface plasmon resonance (SPR) band to more than 570 nm (Figure 6a and Figure S14 in Supporting Information), as compared to the ones observed from monodispersed gold nanoparticles (ca. 520 nm).[27] The shifting of the SPR band in Au@SAC-1 shows a slight difference from that of Au@SAC-2, which was also reflected by the corresponding colors of the dispersions (inset in Figure 6a). Fourier transform infrared spectroscopy (FT-IR) and energy-dispersive X-ray spectrometry (EDS) studies also confirm the formation of gold nanoparticle hybrid superstructures (see the corresponding spectra and discussions in Figures S15 and S16 in Supporting Information).

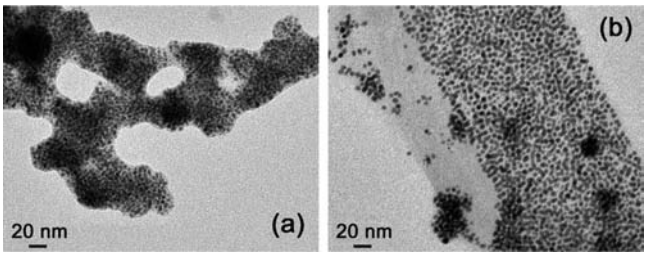

Figure 5. TEM images of (a) Au@SAC-1 and (b) Au@SAC-2, prepared from the corresponding *n*-butanol dispersions.

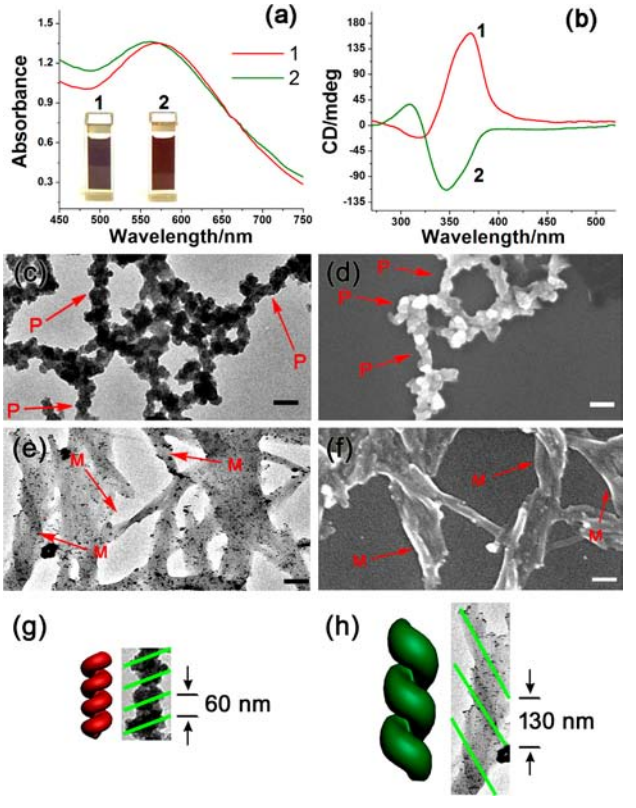

Figure 6. Formation of Au@SAC-1 and Au@SAC-2 and their chirality difference. (a) Absorption spectra (SPR band) of *n*-butanol dispersions of Au@SAC-1 (curve 1) and Au@SAC-2 (curve 2). (Inset) Corresponding photographs of the dispersions. (b) CD spectra of *n*-butanol dispersions of Au@SAC-1 (curve 1) and Au@SAC-2 (curve 2). (c, e) TEM images with relatively large scale for (c) Au@SAC-1 and (e) Au@SAC-2, prepared from the corresponding *n*-butanol dispersions. (d, f) SEM images with relatively large scale for (d) Au@SAC-1 and (f) Au@SAC-2, prepared from the corresponding *n*-butanol dispersions. Some clear helical twists of the nanostructures in panels c−f are highlighted by red arrows. Scale bar = 100 nm. (g, h) Model representations of (g) Au@SAC-1 and (h) Au@SAC-2.

When these nanostructures were further examined by CD spectroscopy, an encouraging phenomenon was observed. Dilute dispersions of the gold nanoparticle superstructures exhibit similar chiral behavior as their corresponding precursors, that is, mixtures of $HAuCl_4$ and the SAC micelle in sol and gel states, respectively (see CD spectra in Figure 6b). The Cotton effect of Au@SAC-2 also reveals a positive−negative pair of peaks at the electronic transition region of the azobenzene unit, while that of Au@SAC-1 displays a negative−positive pair of peaks. These results indicate that the difference in chirality can be preserved with subsequent formation of gold nanoparticle superstructures. Electron microscopy with relatively large scale provides further insight into the chiral character of these superstructures. It can be seen that Au@SAC-1 normally adopts a clockwise helical stacking mode (*P*-helix),[24] whereas Au@SAC-2 exhibits an anticlockwise pattern (*M*-helix)[24] (Figure 6c−f). The pitch in these hierarchical nanoarchitectures of Au@SAC-1 and Au@SAC-2 can also be measured as 60 and 130 nm, respectively (Figure 6g,h). Such pitch difference is in agreement with their cross-sectional diameter difference shown in Figures 5 and 6. These interesting results came from optimization of a series of parallel experiments for preparation of the hybrid nanostructures under different strategies (see Table S3 and Figures S4 and S17 in Supporting Information for details). Although the temperature and addition sequence of the reaction materials can affect the chiral expression, it is clearly demonstrated that chirality control for in situ preparation of the hybrid superstructures can be realized by employing the sol and gel states of SAC as template. In addition, chiroptical properties of the hybrid superstructures in the plasmonic region (~570 nm) were also explored. The CD signals of Au@SAC-1 and Au@SAC-2 around 570 nm are relatively weak as a result of low chiral transfer efficiency in the systems as well as small oscillator strength of the gold nanoparticles.[28] Nevertheless, magnified CD spectra feature the opposite plasmonic signals between Au@SAC-1 and Au@SAC-2 (Figure S18 in Supporting Information).

Solvent Stability of the Superstructures. The chiral appearance of the unimolecular template is largely solvent-dependent, as exemplified in Figure 2. However, such a limitation was well overcome by the formation of gold nanoparticle superstructures. Beyond *n*-butanol, the chirality difference between Au@SAC-1 and Au@SAC-2 can also be observed in several other solvents with different polarities (e.g., toluene, acetone, and water; see the corresponding CD signals in Figure 7). This finding suggests that the whole nanoarchitectures of Au@SAC-1 and Au@SAC-2 remain intact and the inorganic−organic hybrid entities are retained in these media, owing to the immobilization effect generated from the equilibrium between destabilization of the organic components

dx.doi.org/10.1021/ja403722t | J. Am. Chem. Soc. 2013, 135, 9174−9180

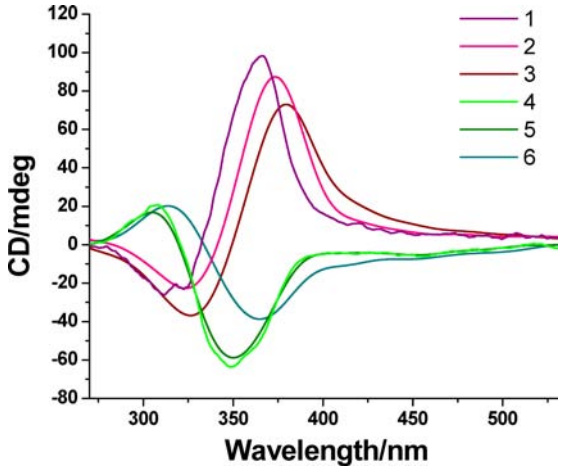

Figure 7. Stability of Au@SAC-1 and Au@SAC-2 in different solvents: CD spectra of Au@SAC-1 in (1) toluene, (2) acetone, and (3) water and of Au@SAC-2 in (4) toluene, (5) acetone, and (6) water.

and the Hamaker attraction of gold nanoparticles.[29] Thus, the solvent stability of the nanoarchitectures is strengthened through a rational combination of the organic component with the gold component. This property broadens the potential application scope of chiral hybrid nanomaterials.

■ CONCLUSION

Chirality control in the in situ preparation of hybrid gold nanoparticle superstructures has been realized via the unimolecular strategy of using a coordinatable organogelator as template. Upon addition of $HAuCl_4$ into the sol form of the template, coordination between the azobenzene moiety and Au(III) leads to chirality inversion of the helical micelles. Upon introduction of $HAuCl_4$ into the gel form, the thickness of the micelles that cannot get enough contact with $HAuCl_4$ prevents the coordination, and thus the original chirality is maintained. After subsequent reduction by TBAB, the chirality difference between the resulting gold nanoparticle superstructures can be preserved and cannot be disrupted in several solvents. These observations have been well supported by multiple experimental characterization techniques as well as by theoretical calculations. The strategy demonstrated herein could thus be valuable for potential exploitation toward the development of smart chiral nanomaterials.

■ EXPERIMENTAL SECTION

General. ^{1}H NMR and ^{13}C NMR spectra were measured on a Bruker BBFO-400 spectrometer. Electronic spray ionization mass spectra were recorded on a ThermoFinnigan LCQ quadrupole ion trap mass spectrometer. High-resolution mass spectrometry (HRMS) was performed on a Waters Q-tof Premier MS spectrometer. Absorption spectra were recorded on a Shimadzu UV-3600 UV−vis−NIR spectrophotometer, while the CD spectra were recorded on a Jasco J-810 CD spectrophotometer. All the optical spectra discussed in this work were determined at a concentration of 0.3 mM calculated from the azobenzene unit in a cuvette with a path length of 1 mm. TEM images were collected on a JEM-1400 (JEOL) operated at 100−120 kV. SEM images were obtained on a JSM 6340 scanning electron microscope (0.5−30 kV) equipped with cold cathode field-emission gun (FEG) as electron source. Energy-dispersive X-ray spectra (EDS) were collected from JED-2300F (JEOL) equipped with SEM of field-emission JSM-6700F (JEOL) operated at 15 kV. FT-IR spectra were recorded on a Shimadzu IR Prestige-21 spectrophotometer. Melting points were determined by use of an OptiMelt automated melting point system. The photo images were photographed by a Nikon Coolpix S8000 digital camera.

Synthesis of Compounds A and SA. These compounds were prepared according to our previous report.[17b]

Synthesis of Compound AC. A solution of cholesteryl chloroformate (0.42 g, 0.93 mmol) in anhydrous acetone (10 mL) was added dropwise into a mixed solution of compound A (0.2 g, 0.93 mmol) and triethylamine (0.1 mL) in anhydrous acetone (20 mL) at room temperature. After the mixture was stirred at room temperature for 16 h, the byproduct quaternary ammonium salt was removed by filtration. The filtrate was concentrated under vacuum, and the residue was washed with ethanol (20 mL) and petroleum ether (5 mL). Then the crude product was purified through silica gel chromatography (petroleum ether:ethyl acetate = 20:1) to afford yellow compound AC (195 mg, 33.6%), mp 148−150 °C. ^{1}H NMR (400 MHz, $CDCl_3$, 298 K) δ = 7.93 (d, J = 8.8 Hz, 2H), 7.89 (d, J = 8.8 Hz, 2H), 7.35 (d, J = 8.8 Hz, 2H), 6.97 (d, J = 8.8 Hz, 2H), 5.44 (s, 1H), 4.62 (m, 1H), 2.48 (m, 1H), 2.04 (m, 1H), 1.59−0.71 (m, 41H). ^{13}C NMR (100 MHz, $CDCl_3$, 298 K) δ = 149.80, 138.50, 125.01, 123.83, 123.75, 123.30, 121.63, 115.81, 83.03, 79.15, 77.22, 56.64, 56.13, 49.93, 42.31, 39.67, 39.52, 37.58, 36.76, 36.50, 36.18, 35.78, 31.89, 31.80, 28.21, 28.02, 27.37, 24.27, 23.83, 22.83, 22.57, 21.04, 19.22, 18.72, 11.86. HRMS (ESI) m/z $[M + H]^+$ calcd for $C_{40}H_{55}N_2O_4$, 627.4162; found, 627.4166.

Synthesis of Compound SAC. A solution of cholesteryl chloroformate (1.26 g, 2.79 mmol) in anhydrous acetone (20 mL) was added dropwise into a mixed solution of SA (585 mg, 1.45 mmol) and triethylamine (0.1 mL) in anhydrous acetone (20 mL) at room temperature. After the mixture was stirred at room temperature for 24 h, the byproduct quaternary ammonium salt was removed by filtration. The filtrate was concentrated under vacuum, and the residue was washed with ethanol (50 mL) and petroleum ether (15 mL). Then the crude product was purified through silica gel chromatography (petroleum ether:ethyl acetate = 40:1) to afford yellow compound SAC (682 mg, 57.7%), mp 131−133 °C. ^{1}H NMR (400 MHz, $CDCl_3$, 298 K) δ = 7.97 (d, J = 8.8 Hz, 4H), 7.36 (d, J = 8.8 Hz, 2H), 7.25 (d, J = 8.8 Hz, 2H), 5.45 (s, 1H), 4.62 (m, 1H), 3.65 (m, 1H), 3.20 (m, 2H), 2.64 (t, J = 7.2 Hz, 2H), 2.49 (m, 2H), 2.04 (m, 1H), 1.90 (m, 1H), 1.82 (m, 2H), 1.59−0.71 (m, 45H). ^{13}C NMR (100 MHz, $CDCl_3$, 298 K) δ = 171.63, 153.03, 152.75, 152.54, 150.14, 139.07, 124.11, 123.31, 122.23, 121.71, 79.19, 77.23, 56.69, 56.30, 56.13, 49.99, 42.33, 40.26, 39.71, 39.52, 38.53, 37.93, 36.84, 36.57, 36.19, 35.79, 34.62, 34.18, 31.92, 31.85, 28.73, 28.23, 28.02, 27.65, 24.60, 24.29, 23.83, 22.83, 22.57, 21.06, 19.30, 18.72, 11.87. HRMS (ESI) m/z $[M + H]^+$ calcd for $C_{48}H_{67}N_2O_5S_2$, 815.4491; found, 815.4503.

Gelation Test in Different Organic Solvents. SAC (10 mg) and different solvents (0.5 mL) were placed in a capped vial, which was heated until the solid was dissolved (SAC cannot be entirely dissolved in some solvents even by heating). Then the solution was cooled naturally to room temperature. In our study, we found that only n-butanol can be effectively gelated by SAC. Once the gel was formed, it can be reversibly transformed between the gel and sol states by heating and cooling, respectively. For a batch sol−gel system with 0.5 wt % SAC, the gel-to-sol transition temperature is 52 °C.

Preparation of Au@SAC-1. SAC (4.0 mg) and n-butanol (0.8 mL) were placed in a capped vial, which was heated until the solid was entirely dissolved. The mixture was cooled to 55 °C and remained as a fluid sol under stirring. Then $HAuCl_4$ (8 mg) in n-butanol (0.2 mL) was added into the sol, immediately accompanied by an obvious color change of the mixture from yellow to red. After Au(III) was reduced by the addition of tetrabutylammonium borohydride (TBAB, 2.4 mg) in n-butanol (0.2 mL), the mixture was kept stirring for another 20 min. The resulted hybrid gold nanostructure Au@SAC-1 was isolated by centrifugation (1500 rpm, 15 min) and washed by n-butanol to sufficiently remove free ligand and excessive reagents. Au@SAC-1 was either dried under vacuum or redispersed in different solvents for further investigations.

Preparation of Au@SAC-2. SAC (4.0 mg) and n-butanol (0.8 mL) were placed in a capped vial, which was heated until the solid was entirely dissolved. The mixture was cooled to room temperature and

became the gel state. The gel was minced under stirring for better interactions with additional agents. Then $HAuCl_4$ (8 mg) in *n*-butanol (0.2 mL) was added to the minced gel, and only the surface color of the micelles slightly turned red. TBAB (2.4 mg) in *n*-butanol (0.2 mL) was added under manual stirring for the Au(III) reduction, and the resulting mixture was kept stirring for another 20 min. The obtained hybrid gold nanostructure Au@SAC-2 was isolated by centrifugation (1500 rpm, 15 min) and washed by *n*-butanol to sufficiently remove free ligand and excessive reagents. Au@SAC-2 was either dried under vacuum or redispersed in different solvents for further investigations.

Computational Details. The geometries of compounds SAC and 2Au(III)−SAC were optimized by density functional theory calculations employing the hybrid B3LYP functional[30] and the 6-31G* basis set[31] as implemented in the Gaussian 09 program.[32] For gold atoms in 2Au(III)−SAC, the Los Alamos effective core potential basis set (LANL2DZ)[33] was used. At the optimized geometry, the electrostatic potential (ESP) was calculated at the Hartree−Fock level of theory according to the Merz−Singh−Kollman scheme.[34] Atomic partial charges for subsequent molecular dynamics (MD) simulations were derived on the basis of the restrained electrostatic potential (RESP).[35] The general Amber force field (GAFF)[36] was employed to model the organic part of the molecules, and the Hess2FF scheme[37] was used to derive force field parameters for bonded interaction involving gold atoms. Here, the equilibrium bond lengths and bond angles as well as the force constants for dihedral potentials were further refined so that the molecular mechanical force field could well reproduce the quantum chemically predicted geometries. The Lennard-Jones parameters for gold atoms were adopted from literature.[38] MD simulations were carried out with the GROMACS program package.[25] For each compound, 10 molecules were solvated in TIP3P water[39] and simulated under constant-*NpT* conditions (T = 298 K, p = 1 atm) for 50 ns. For comparison, simulations of SAC molecules were also performed in methanol for 65 ns. Snapshots were extracted from each simulation trajectory with an equal interval of 500 ps, and the computed electronic circular dichroism (ECD) spectra were averaged over snapshots of the last 10 ns. The semiempirical ZIndo/S method[40] and time-dependent density functional theory (TDDFT) calculations with the PBE0 functional[41] were employed to compute the ECD spectra.

■ ASSOCIATED CONTENT

Supporting Information

Additional text, 18 figures, and three tables describing cac and cmc measurements for SAC, observations for cgc, coordination studies between SAC and Au(III), complexation constant K between SAC and $HAuCl_4$, supplementary computational results and characterizations of superstructures, optimization for in situ preparation strategy, and full citation for ref 32. This material is available free of charge via the Internet at http://pubs.acs.org.

■ AUTHOR INFORMATION

Corresponding Author

zhaoyanli@ntu.edu.sg

Author Contributions

[§]L.Z. and X.L. contributed equally.

Notes

The authors declare no competing financial interest.

■ ACKNOWLEDGMENTS

This work was financially supported by the Singapore National Research Foundation Fellowship (NRF2009NRF-RF001-015), the Singapore National Research Foundation CREATE program−Singapore Peking University Research Centre for a Sustainable Low-Carbon Future, and the Centre of Excellence for Silicon Technologies (A*Star SERC 112 351 0003). L.Z. thanks C. Y. Ang, Z.-N. Liu, Z. Luo, X. Ma, X. Yao, M.-H. Li, and L.-Y. Bai for helpful discussions. X.L. acknowledges a grant from the Carl Tryggers Foundation and computational resources provided by the Swedish National Infrastructure for Computing under the project Multiphysics Modeling of Molecular Materials, SNIC 022/09-25.

■ REFERENCES

(1) (a) Whitesides, G. M.; Grzybowski, B. *Science* **2002**, *295*, 2418−2421. (b) Kinbara, K.; Aida, T. *Chem. Rev.* **2005**, *105*, 1377−1400. (c) Lehn, J. M. *Science* **2002**, *295*, 2400−2403. (d) Aida, T.; Meijer, E. W.; Stupp, S. I. *Science* **2012**, *335*, 813−817. (e) Kiyonaka, S.; Sada, K.; Yoshimura, I.; Shinkai, S.; Kato, N.; Hamachi, I. *Nat. Mater.* **2004**, *3*, 58−64. (f) Valev, V. K.; Baumberg, J. J.; Sibilia, C.; Verbiest, T. *Adv. Mater.* **2013**, *25*, 2517−2534.

(2) (a) Kondo, Y.; Takayanagi, K. *Science* **2000**, *289*, 606−608. (b) Wu, Y.; Cheng, G.; Katsov, K.; Sides, S. W.; Wang, J.; Tang, J.; Fredrickson, G. H.; Moskovits, M.; Stucky, G. D. *Nat. Mater.* **2004**, *3*, 816−822. (c) Shopsowitz, K. E.; Qi, H.; Hamad, W. Y.; MacLachlan, M. J. *Nature* **2010**, *468*, 422−425. (d) Zhu, J.; Peng, H.; Marshall, A. F.; Barnett, D. M.; Nix, W. D.; Cui, Y. *Nat. Nanotechnol.* **2008**, *3*, 477−481. (e) Zhou, Y.; Yang, M.; Sun, K.; Tang, Z.; Kotov, N. A. *J. Am. Chem. Soc.* **2010**, *132*, 6006−6013. (f) Thomas, J. M.; Raja, R. *Acc. Chem. Res.* **2008**, *41*, 708−720. (g) Gabashvili, A.; Medina, D. D.; Gedanken, A.; Mastai, Y. *J. Phys. Chem. B* **2007**, *111*, 11105−11110. (h) Fireman-Shoresh, S.; Popov, I.; Avnir, D.; Marx, S. *J. Am. Chem. Soc.* **2005**, *127*, 2650−2655. (i) Hodgkinson, I.; Wu, Q. H. *Adv. Mater.* **2001**, *13*, 889−897. (j) Kong, X. Y.; Wang, Z. L. *Nano Lett.* **2003**, *3*, 1625−1631.

(3) (a) Qiu, H.; Che, S. *Chem. Soc. Rev.* **2011**, *40*, 1259−1268. (b) Yang, X.; Tang, H.; Cao, K.; Song, H.; Sheng, W.; Wu, Q. *J. Mater. Chem.* **2011**, *21*, 6122−6135. (c) Wang, Y.; Xu, J.; Wang, Y.; Chen, H. *Chem. Soc. Rev.* **2013**, *42*, 2930−2962.

(4) (a) Slocik, J. M.; Govorov, A. O.; Naik, R. R. *Nano Lett.* **2011**, *11*, 701−705. (b) Chen, C.-L.; Rosi, N. L. *Angew. Chem., Int. Ed.* **2010**, *49*, 1924−1942.

(5) (a) Li, Z.; Zhu, Z.; Liu, W.; Zhou, Y.; Han, B.; Gao, Y.; Tang, Z. *J. Am. Chem. Soc.* **2012**, *134*, 3322−3325. (b) Shemer, G.; Krichevski, O.; Markovich, G.; Molotsky, T.; Lubitz, I.; Kotlyar, A. B. *J. Am. Chem. Soc.* **2006**, *128*, 11006−11007.

(6) (a) Delclos, T.; Aimé, C.; Pouget, E.; Brizard, A.; Huc, I.; Delville, M.-H.; Oda, R. *Nano Lett.* **2008**, *8*, 1929−1935. (b) Wang, R.-Y.; Wang, H.; Wu, X.; Ji, Y.; Wang, P.; Qu, Y.; Chung, T.-S. *Soft Matter* **2011**, *7*, 8370−8375. (c) Yokoi, T.; Ogawa, K.; Lu, D.; Kondo, J. N.; Kubota, Y.; Tatsumi, T. *Chem. Mater.* **2011**, *23*, 2014−2016. (d) Jin, H.; Liu, Z.; Ohsuna, T.; Terasaki, O.; Inoue, Y.; Sakamoto, K.; Nakanishi, T.; Ariga, K.; Che, S. *Adv. Mater.* **2006**, *18*, 593−596.

(7) (a) Jung, J. H.; Lee, S.-H.; Yoo, J. S.; Yoshida, K.; Shimizu, T.; Shinkai, S. *Chem.—Eur. J.* **2003**, *9*, 5307−5313. (b) Llusar, M.; Sanchez, C. *Chem. Mater.* **2008**, *20*, 782−820.

(8) To mention a few examples: (a) Chen, W.; Bian, A.; Agarwal, A.; Liu, L.; Shen, H.; Wang, L.; Xu, C.; Kotov, N. A. *Nano Lett.* **2009**, *9*, 2153−2159. (b) Oh, H. S.; Liu, S.; Jee, H.; Baev, A.; Swihart, M. T.; Prasad, P. N. *J. Am. Chem. Soc.* **2010**, *132*, 17346−17348. (c) Tseng, W.-H.; Chen, C.-K.; Chiang, Y.-W.; Ho, R.-M.; Akasaka, S.; Hasegawa, H. *J. Am. Chem. Soc.* **2009**, *131*, 1356−1357. (d) Karatchevtseva, I.; Cassidy, D. J.; Man, M. W. C.; Mitchell, D. R. G.; Hanna, J. V.; Carcel, C.; Bied, C.; Moreau, J. J. E.; Bartlett, J. R. *Adv. Funct. Mater.* **2007**, *17*, 3926−3932.

(9) (a) Li, C.; Deng, K.; Tang, Z.; Jiang, L. *J. Am. Chem. Soc.* **2010**, *132*, 8202−8209. (b) George, J.; Thomas, K. G. *J. Am. Chem. Soc.* **2010**, *132*, 2502−2503.

(10) (a) Chen, Q.; Whitmer, J. K.; Jiang, S.; Bae, S. C.; Luijten, E.; Granick, S. *Science* **2011**, *331*, 199−202. (b) Gautier, C.; Bürgi, T. *J. Am. Chem. Soc.* **2008**, *130*, 7077−7084. (c) Wang, H.; Wu, J.-C.; Shen, Y.; Li, G.; Zhang, Z.; Xing, G.; Guo, D.; Wang, D.; Dong, Z.; Wu, T. *J. Am. Chem. Soc.* **2010**, *132*, 15875−15877.

(11) (a) Huang, Z.; Kang, S.-K.; Banno, M.; Yamaguchi, T.; Lee, D.; Seok, C.; Yashima, E.; Lee, M. *Science* **2012**, *337*, 1521−1526. (b) Zhang, Y.; O'Callaghan, M. J.; Baumeister, U.; Tschierske, C. *Angew. Chem., Int. Ed.* **2008**, *47*, 6892−6896. (c) Gopal, A.; Hifsudheen, M.; Furumi, S.; Takeuchi, M.; Ajayaghosh, A. *Angew. Chem., Int. Ed.* **2012**, *51*, 10505−10509. (d) Peterca, M.; Imam, M. R.; Ahn, C.-H.; Balagurusamy, V. S. K.; Wilson, D. A.; Rosen, B. M.; Percec, V. *J. Am. Chem. Soc.* **2011**, *133*, 2311−2328. (e) Lohr, A.; Würthner, F. *Chem. Commun.* **2008**, 2227−2229. (f) Moriyama, M.; Mizoshita, N.; Yokota, T.; Kishimoto, K.; Kato, T. *Adv. Mater.* **2003**, *15*, 1335−1338.

(12) (a) Crassous, J. *Chem. Commun.* **2012**, *48*, 9684−9692. (b) Ousaka, N.; Takeyama, Y.; Yashima, E. *Chem. Sci.* **2012**, *3*, 466−469. (c) Shin, S.; Lim, S.; Kim, Y.; Kim, T.; Choi, T.-L.; Lee, M. *J. Am. Chem. Soc.* **2013**, *135*, 2156−2159.

(13) (a) Zhao, Y. L.; Aprahamian, I.; Trabolsi, A.; Erina, N.; Stoddart, J. F. *J. Am. Chem. Soc.* **2008**, *130*, 6348−6350. (b) Wang, S.; Shen, W.; Feng, Y.; Tian, H. *Chem. Commun.* **2006**, 1497−1499. (c) Klawonn, T.; Gansäuer, A.; Winkler, I.; Lauterbach, T.; Franke, D.; Nolte, R. J. M.; Feiters, M. C.; Börner, H.; Hentschel, J.; Dötz, K. H. *Chem. Commun.* **2007**, 1894−1895.

(14) (a) Zhu, L.; Yan, H.; Wang, X.-J.; Zhao, Y. L. *J. Org. Chem.* **2012**, *77*, 10168−10175. (b) Zhu, L.; Yan, H.; Ang, C. Y.; Nguyen, K. T.; Li, M.; Zhao, Y. L. *Chem.—Eur. J.* **2012**, *18*, 13979−13983. (c) Zhu, L.; Lu, M.; Qu, D.; Wang, Q.; Tian, H. *Org. Biomol. Chem.* **2011**, *9*, 4226−4233.

(15) (a) Willner, I.; Pardo-Yissar, V.; Katz, E.; Ranjit, K. T. *J. Electroanal. Chem.* **2001**, *497*, 172−177. (b) Chiu, K. Y.; Tu, Y.-J.; Lee, C.-J.; Yang, T.-F.; Lai, L.-L.; Chao, I.; Su, Y. O. *Electrochim. Acta.* **2012**, *62*, 51−62.

(16) (a) Ghedini, M.; Aiello, I.; Crispini, A.; Golemme, A.; Deda, M. L.; Pucci, D. *Coord. Chem. Rev.* **2006**, *250*, 1373−1390. (b) Omae, I. *Coord. Chem. Rev.* **2011**, *255*, 139−160. (c) Wang, H.; Bao, C.; Li, F.; Kong, X.; Xu, J. *Microchim. Acta* **2010**, *168*, 99−105.

(17) (a) Sperling, R. A.; Parak, W. J. *Philos. Trans. R. Soc. London, Ser. A* **2010**, *368*, 1333−1383. (b) Zhu, L.; Yan, H.; Nguyen, K. T.; Tian, H.; Zhao, Y. L. *Chem. Commun.* **2012**, *48*, 4290−4292. (c) Zhu, L.; Ang, C. Y.; Li, X.; Nguyen, K. T.; Tan, S. Y.; Ågren, H.; Zhao, Y. L. *Adv. Mater.* **2012**, *24*, 4020−4024.

(18) Gautier, C.; Bürgi, T. *ChemPhysChem* **2009**, *10*, 483−492.

(19) (a) Wang, L.; Xu, L.; Kuang, H.; Xu, C.; Kotov, N. A. *Acc. Chem. Res.* **2012**, *45*, 1916−1926. (b) Fafarman, A. T.; Hong, S.-H.; Caglayan, H.; Ye, X.; Diroll, B. T.; Paik, T.; Engheta, N.; Murray, C. B.; Kagan, C. R. *Nano Lett.* **2013**, *13*, 350−357.

(20) (a) Berova, N.; Bari, L. D.; Pescitelli, G. *Chem. Soc. Rev.* **2007**, *36*, 914−931. (b) Canary, J. W. *Chem. Soc. Rev.* **2009**, *38*, 747−756.

(21) (a) Jain, N.; Trabelsi, S.; Guillot, S.; McLoughlin, D.; Langevin, D.; Letellier, P.; Turmine, M. *Langmuir* **2004**, *20*, 8496−8503. (b) Okuzaki, H.; Osada, Y. *Macromolecules* **1995**, *28*, 380−382.

(22) (a) Estroff, L. A.; Hamilton, A. D. *Chem. Rev.* **2004**, *104*, 1201−1217. (b) Svobodová, H.; Noponen, V.; Kolehmainen, E.; Sievänen, E. *RSC Adv.* **2012**, *2*, 4985−5007. (c) Zhu, L.; Ma, X.; Ji, F.; Wang, Q.; Tian, H. *Chem.—Eur. J.* **2007**, *13*, 9216−9222. (d) Wang, X.-J.; Xing, L.-B.; Cao, W.-N.; Li, X.-B.; Chen, B.; Tung, C.-H.; Wu, L.-Z. *Langmuir* **2011**, *27*, 774−781. (e) de Loos, M.; Feringa, B. L.; van Esch, J. H. *Eur. J. Org. Chem.* **2005**, *70*, 3615−3631. (f) Gao, P.; Zhan, C. L.; Liu, M. H. *Langmuir* **2006**, *22*, 775−779.

(23) (a) Murata, K.; Aoki, M.; Suzuki, T.; Harada, T.; Kawabata, H.; Komori, T.; Ohseto, F.; Ueda, K.; Shinkai, S. *J. Am. Chem. Soc.* **1994**, *116*, 6664−6676. (b) Cui, J.; Liu, A.; Guan, Y.; Zheng, J.; Shen, Z.; Wan, X. *Langmuir* **2010**, *26*, 3615−3622.

(24) (a) Lu, X.; Guo, Z.; Sun, C.; Tian, H.; Zhu, W. *J. Phys. Chem. B* **2011**, *115*, 10871−10876. (b) Danila, I.; Riobé, F.; Piron, F.; Puigmartí-Luis, J.; Wallis, J. D.; Linares, M.; Ågren, H.; Beljonne, D.; Amabilino, D. B.; Avarvari, N. *J. Am. Chem. Soc.* **2011**, *133*, 8344−8353. (c) Zhu, L.; Li, X.; Zhang, Q.; Ma, X.; Li, M.; Zhang, H.; Luo, Z.; Ågren, H.; Zhao, Y. L. *J. Am. Chem. Soc.* **2013**, *135*, 5175−5182.

(25) Hess, B.; Kutzner, C.; van der Spoel, D.; Lindahl, E. *J. Chem. Theory Comput.* **2008**, *4*, 435−447.

(26) Mayoral, M. J.; Rest, C.; Stepanenko, V.; Schellheimer, J.; Albuquerque, R. Q.; Fernández, G. *J. Am. Chem. Soc.* **2013**, *135*, 2148−2151.

(27) Jana, N. R.; Gearheart, L.; Murphy, C. J. *Langmuir* **2001**, *17*, 6782−6786.

(28) (a) Kuzyk, A.; Schreiber, R.; Fan, Z.; Pardatscher, G.; Roller, E.-M.; Högele, A.; Simmel, F. C.; Govorov, A. O.; Liedl, T. *Nature* **2012**, *483*, 311−314. (b) Shen, X.; Song, C.; Wang, J.; Shi, D.; Wang, Z.; Liu, N.; Ding, B. *J. Am. Chem. Soc.* **2012**, *134*, 146−149. (c) Zhu, Z.; Liu, W.; Li, Z.; Han, B.; Zhou, Y.; Gao, Y.; Tang, Z. *ACS Nano* **2012**, *6*, 2326−2332.

(29) (a) Jin, Q.; Xu, J.-P.; Ji, J.; Shen, J.-C. *Chem. Commun.* **2008**, 3058−3060. (b) Zhang, H.; Wang, D. *Angew. Chem., Int. Ed.* **2008**, *47*, 3984−3987.

(30) (a) Becke, A. D. *J. Chem. Phys.* **1993**, *98*, 5648−5652. (b) Stephens, P. J.; Devlin, F. J.; Chabalowski, C. F.; Frisch, M. J. *J. Phys. Chem.* **1994**, *98*, 11623−11627.

(31) Hehre, W. J.; Ditchfield, R.; Pople, J. A. *J. Chem. Phys.* **1972**, *56*, 2257−2261.

(32) Frisch, M. J.; et al. *Gaussian 09*, Revision A.2; Gaussian, Inc., Wallingford, CT, 2009.

(33) Hay, P. J.; Wadt, W. R. *J. Chem. Phys.* **1985**, *82*, 270−283.

(34) (a) Singh, U. C.; Kollman, P. A. *J. Comput. Chem.* **1984**, *5*, 129−145. (b) Besler, B. H.; Merz, K. M., Jr.; Kollman, P. A. *J. Comput. Chem.* **1990**, *11*, 431−439.

(35) Bayly, C. I.; Cieplak, P.; Cornell, W.; Kollman, P. A. *J. Phys. Chem.* **1993**, *97*, 10269−10280.

(36) (a) Wang, J.; Wolf, R. M.; Caldwell, J. W.; Kollman, P. A.; Case, D. A. *J. Comput. Chem.* **2004**, *25*, 1157−1174. (b) Duchstein, P.; Neiss, C.; Görling, A.; Zahn, D. *J. Mol. Model.* **2012**, *18*, 2479−2482.

(37) (a) Seminario, J. M. *Int. J. Quantum Chem.* **1996**, *60*, 1271−1277. (b) Nilsson, K.; Lecerof, D.; Sigfridsson, E.; Ryde, U. *Acta Crystallogr. D* **2003**, *59*, 274−289.

(38) Schoen, P. A. E.; Walther, J. H.; Arcidiacono, S.; Poulikakos, D.; Koumoutsakos, P. *Nano Lett.* **2006**, *6*, 1910−1917.

(39) Jorgensen, W. L.; Chandrasekhar, J.; Madura, J. D.; Impey, R. W.; Klein, M. L. *J. Chem. Phys.* **1983**, *79*, 926−935.

(40) Zerner, M. C. In *Reviews of Computational Chemistry*; Lipkowitz, K. B., Boyd, D. B., Eds.; VCH Publishing: New York, 1991; Vol. *2*, pp 313−366.

(41) Adamo, C.; Barone, V. *J. Chem. Phys.* **1999**, *110*, 6158−6169.